Recycling endosomes can serve as intermediates during transport from the Golgi to the plasma membrane of MDCK cells

Agnes Lee Ang, Tomohiko Taguchi, Stephen Francis, Heike Fölsch, Lindsay J. Murrells, Marc Pypaert, Graham Warren, and Ira Mellman

Department of Cell Biology, Ludwig Institute for Cancer Research, Yale University School of Medicine, New Haven, CT 06520

The AP-1B clathrin adaptor complex is responsible for the polarized transport of many basolateral membrane proteins in epithelial cells. Localization of AP-1B to recycling endosomes (REs) along with other components (exocyst subunits and Rab8) involved in AP-1B–dependent transport suggested that RE might be an intermediate between the Golgi and the plasma membrane. Although the involvement of endosomes in the secretory pathway has long been suspected, we now present direct evidence using four independent methods that REs play a role in basolateral transport in MDCK cells. Newly synthe-sized AP-1B–dependent cargo, vesicular stomatitis virus glycoprotein G (VSV-G), was found by video microscopy, immunoelectron microscopy, and cell fractionation to en-ter transferrin-positive REs within a few minutes after exit from the trans-Golgi network. Although transient, RE entry appears essential because enzymatic inactivation of REs blocked VSV-G delivery to the cell surface. Because an apically targeted VSV-G mutant behaved similarly, these results suggest that REs not only serve as an intermediate but also as a common site for polarized sorting on the endocytic and secretory pathways.

Introduction

Polarized epithelial cells have the ability to generate and maintain biochemically distinct apical and basolateral plasma membrane domains (Drubin and Nelson, 1996; Mostov et al., 2000). Proteins in the exocytic and endocytic pathways are tar-geted to their correct domains after segregation of apical and basolateral proteins into distinct transport carriers. Lumenal carbohydrate moieties or lipid binding properties of transmem-brane anchors are often important for inclusion in apical carriers. In contrast, sorting of membrane proteins into basolateral carriers typically depends on the recognition of discrete cytoplasmic domain targeting signals. These signals often involve tyrosine or dileucine motifs, many of which are recognized by clathrin adaptor complexes (Bonifacino and Traub, 2003). Of particular importance is the epithelial cell-specific AP-1B adaptor, essen-tial for the basolateral expression of numerous membrane proteins including vesicular stomatitis virus glycoprotein G (VSV-G), transferrin receptor (TfnR), asialoglycoprotein re-ceptor, and low density lipoprotein receptor (Fölsch et al., 1999, 2003; Ohno et al., 1999; Sugimoto et al., 2002). The ex-act site or sites at which AP-1B deciphers basolateral targeting signals has not yet been defined, although it is highly likely that AP-1B mediates sorting in the perinuclear region possibly at the TGN or endosomes (Fölsch et al., 2001; Gan et al., 2002; Ang et al., 2003).

For two decades, the TGN has been the presumed sorting site for all newly synthesized membrane and secretory proteins. Evidence for this has been based on a variety of experiments all yielding results consistent with the segregation of cargoes upon exit from the TGN (Rindler et al., 1985; Griffiths and Simons, 1986; Wandinger-Ness et al., 1990; Hirschberg et al., 1998; Keller et al., 2001). However, such data could not exclude the possibility that at least some sorting occurred in recycling endosomes (REs), a complex of vesicles and tubules often located close to the TGN. In epithelial cells, REs appear to sort internalized plasma membrane proteins during recycling (Sheff et al., 1999), relying on much the same signal motifs as are responsible for targeting proteins on the biosynthetic path-way (Matter et al., 1992; Futter et al., 1995; Odorizzi et al., 1996; Sheff et al., 1999). The AP-1B adaptor complex has been localized to REs, together with basolateral cargo and

components of the exocyst complex (Fölsch et al., 2001, 2003; Gan et al., 2002), which are thought to be required for the tethering of transport carriers to the basolateral plasma membrane (Grindstaff et al., 1998; Yeaman et al., 2001). Similarly, the Rab8 GTPase, which regulates the traffic of newly synthesized AP-1B–dependent cargo, was also localized to transferrin (Tfn)-positive REs (Ang et al., 2003). Together, these data suggest that AP-1B–dependent sorting may actually occur in RE (Traub and Apodaca, 2003).

There have been previous suggestions from both mammalian and yeast cells that secretory traffic can, at least to some extent, traverse endocytic compartments on route to the plasma membrane (Hedman et al., 1987; Stoorvogel et al., 1988; Futter et al., 1995; Leitinger et al., 1995; Odorizzi et al., 1996; Orzech et al., 2000; Harsay and Schekman, 2002). With the exception of the yeast work, these important studies did not establish the physiological or quantitative importance of a possible endosomal intermediate; nor did they identify the nature of the endosome compartment(s) involved. Given recent findings that components functionally important for basolateral transport are associated with REs rather than with the TGN, we explored the role of REs on the secretory pathway in MDCK cells in detail.

Results

VSV-G localizes to Tfn-positive compartments after exit from the Golgi complex

We first sought to visualize the possible entry of an AP-1B–dependent membrane protein into Tfn-positive (Tfn+) structures by fluorescence microscopy. We reasoned that residence of newly synthesized proteins in REs was likely to be evanescent, and thus we optimized several conditions to increase chances of visualizing the event. First, an MDCK cell line stably expressing the human TfnR (MDCKT) was used because uptake of human Tfn, fluorescently labeled or epitope-tagged, was >10-fold more efficient than via the endogenous canine receptor (Sheff et al., 1999; unpublished data). Previous work relied only on endogenous TfnR. Second, incubation times and temperatures were regulated to synchronize a pulse of secretory and endocytic cargo, maximizing their possibility of encounter. VSV-G ts045 was used as a reporter and subjected to two sequential temperature blocks, first at 40°C (to accumulate VSV-G in the ER) and next for 2 h at 20°C (to release the ER block and allow accumulation in the TGN; Griffiths et al., 1985). During the 20°C incubation, the cells were allowed to take up Alexa 546–tagged human Tfn, conditions which allow for its accumulation in RE (Sheff et al., 1999). The 20°C block was then released for various periods by shifting to 31°C, a temperature that allowed rapid exit of VSV-G from the TGN but at a rate slower than had the temperature been shifted to 32.5°C or 37°C as is more commonly used. The tagged Tfn was maintained or removed during the 31°C chase with equivalent results.

Initial experiments relied on immunofluorescence microscopy of fixed, coverslip-grown MDCKT cells. A recombinant adenovirus was used to express YFP-tagged ts045 VSV-G,

with cells exposed to a pulse of virus and then incubated overnight at 40°C before shifting to 20°C in the presence of Alexa 546-Tfn. As shown in Fig. 1 A, VSV-G (Fig. 1, green) and Tfn (Fig. 1, red) did not colocalize during the 20°C block. Tfn was localized to a characteristic tight perinuclear cluster (Fig. 1 A, arrows), whereas VSV-G, also in the perinuclear region, was found in largely distinct structures that in many examples appeared to circumscribe the RE. These VSV-G–containing structures colocalized instead with markers of the Golgi such as GM130 (Fölsch et al., 2001) and furin (unpublished data). However, upon shifting to 31°C for 5–10 min and immediately processing the cells for immunofluorescence, VSV-G was observed to be spatially localized with Tfn (Fig. 1 B, arrows) in the Tfn-positive cluster previously devoid of VSV-G. The apparent colocalization of VSV-G and Tfn did not reflect a superimposition of distinct structures in different focal planes as it was evident throughout the entire volume of three-dimensional renderings (Fig. 1, C and D; and Videos 1 and 2, available at http://www.jcb.org/cgi/content/full/jcb.200408165/DC1). Such overlap of VSV-G with Tfn was not observed using cells not expressing human TfnR, due to a much lower labeling efficiency of Tfn and thus inefficient ascertainment of Tfn-containing structures (unpublished data).

Because incubation at 20°C might alter the organization of the Golgi complex, we asked if we could detect an overlap between VSV-G and Tfn by shifting the 40°C cells directly to 31°C. 20–30 min after the shift, some regional colocalization was observed, although far less than if the 20°C block was used (Fig. S1, available at http://www.jcb.org/cgi/content/full/jcb.200408165/DC1). Although this may mean that colocalization partly reflected a temperature-induced reorganization of Golgi or RE elements, eliminating the 20°C step can also be expected to render VSV-G transport more asynchronous. Loss of synchrony results from the time required for refolding of VSV-G before ER exit and from its subsequent transit through the Golgi stack. In any event, these results raised the possibility that some fraction of newly synthesized VSV-G might be transported to RE upon exit from the TGN. We turned to exploring this possibility in detail.

VSV-G is transported to and from REs as visualized by live cell imaging

We monitored the dynamics of VSV-G transport relative to Tfn+ REs by live cell imaging. Cells prepared as in Fig. 1 A were imaged using confocal microscopy every 7 s immediately upon shifting from 20 to 31°C. These results are best viewed by video (Videos 3–7, available at http://www.jcb.org/cgi/content/full/jcb.200408165/DC1) because one can appreciate the multiple green VSV-G–positive (VSV-G+) structures that move centripetally toward the more centrally located red Tfn+ structures. The Tfn+ structures become progressively yellow over time of chase (2–3 min).

In static images taken from the video data, Fig. 2 A illustrates one example of VSV-G+ carriers (Fig. 2 A, green, arrows) moving toward and into a region containing a large Tfn+ structure (Fig. 2 A, red, carrot). VSV-G was first detected as a large vesicular structure (Fig. 2 A, asterisk) that be-
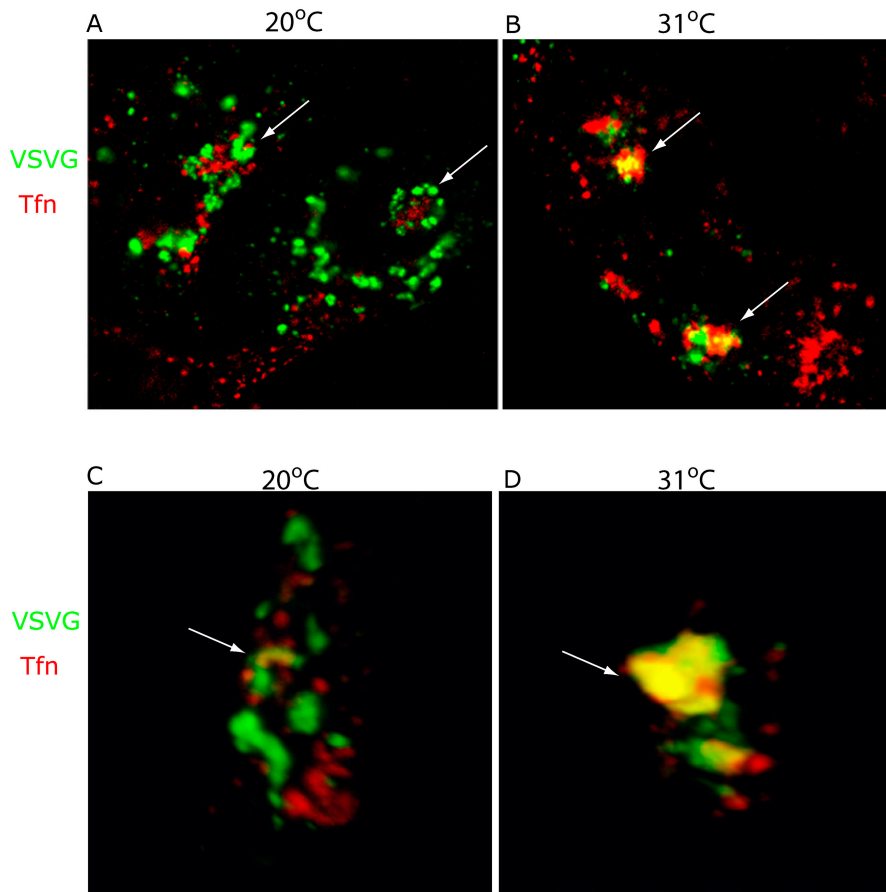
Figure 1. **VSV-G localizes to Tfn-positive membranes after exit from the Golgi complex.** (A) MDCKT cells were infected with ts045 VSV-G-YFP and induced to express transferrin receptor (TfnR). Cells were incubated 2 h at 20°C (last hour in media plus CHX) to accumulate a synchronous pulse of VSV-G (green) at the TGN, and allowed to take up Alexa 546-Tfn (red) into REs. Cells were fixed and imaged. Arrows, REs. (B) Cells in A were released from the TGN block by incubation at 31°C in media plus CHX for 10 min, and then fixed and imaged. Arrows denote colocalization of VSV-G and Tfn (yellow). (C and D) Three-dimensional reconstruction of confocal serial sections, X-Y plane and sagittal section through REs (arrow) of representative cells in A and B.

came tubular, eventually breaking up into smaller vesicular structures, at least some of which clearly proceeded into the large Tfn+ structure (Fig. 2 A, last panel, carrot). Although this phenomenon of tubular and vesicular transport of VSV-G has been previously described in MDCK cells, such colocalization VSV-G with Tfn+ membranes was not readily observed (Keller et al., 2001). Fig. 2 B summarizes the pathway of the VSV-G carrier denoted by the arrow in Fig. 2 A as it progressed from the periphery (Fig. 2 B, purple dots). Over time, the Tfn+ structures increased in yellow fluorescence due to increased spatial colocalization with VSV-G (Fig. 2 A, compare carrots in first and last frames; Video 3). Similar data were obtained using cells expressing an apical variant of VSV-G (Keller et al., 2001), suggesting that both basolateral and apical plasma membrane proteins were targeted to the RE region (Video 5).

Starting after 5 min at 31°C, VSV-G sometimes together with Tfn began to exit the RE region. This is illustrated in Video 6, with a single example shown as static images in Fig. 2 (C and D). VSV-G initially colocalized with Tfn (Fig. 2 C, top, yellow, arrows), exiting the Tfn+ region as a tubule that then appeared to break up into smaller vesicular structures. These structures moved away from the RE region (Fig. 2 D) in a fashion that appeared the reverse of VSV-G entry. Again, similar results were found for the apical variant of VSV-G (Keller et al., 2001), suggesting that transport through the RE region was not exclusive to basolateral cargo (unpublished data).

Although the video images were of too low resolution to ensure that the VSV-G and Tfn were in the same membrane compartments, analysis of VSV-G and Tfn+ structures in the cell periphery suggested that this was the case. As shown in Fig. 2 E and Video 7, there was a close and persistent (1–2 min) association between many green and red elements (Fig. 2 E, arrows), supporting the idea that VSV-G and Tfn-containing structures were fused or at least physically linked.

Thus, real-time imaging of live cells suggested that there was a transient association of VSV-G+ structures and Tfn-containing RE shortly after VSV-G exit from the TGN. That this association occurred on the biosynthetic pathway was suggested by the fact that it was seen only transiently, within 5–10 min after releasing the 20°C block and well before the detection of VSV-G at the plasma membrane (not visible until >30 min of chase, see Video 3). Because both basolateral and apical forms of VSV-G behaved similarly, it further appeared possible that sorting might occur at that site. However, of primary importance was to determine if secretory and endocytic cargo ever actually entered the same membrane-bound structures.

VSV-G and Tfn colocalize in endosomes

To examine the distribution of VSV-G relative to Tfn at higher resolution, we performed EM-immunocytochemistry on MD-CKT cells incubated with Alexa 488-Tfn either before or after shifting from 20 to 31°C. To ensure that detection of VSV-G and Tfn at the EM level was as similar as possible to the live
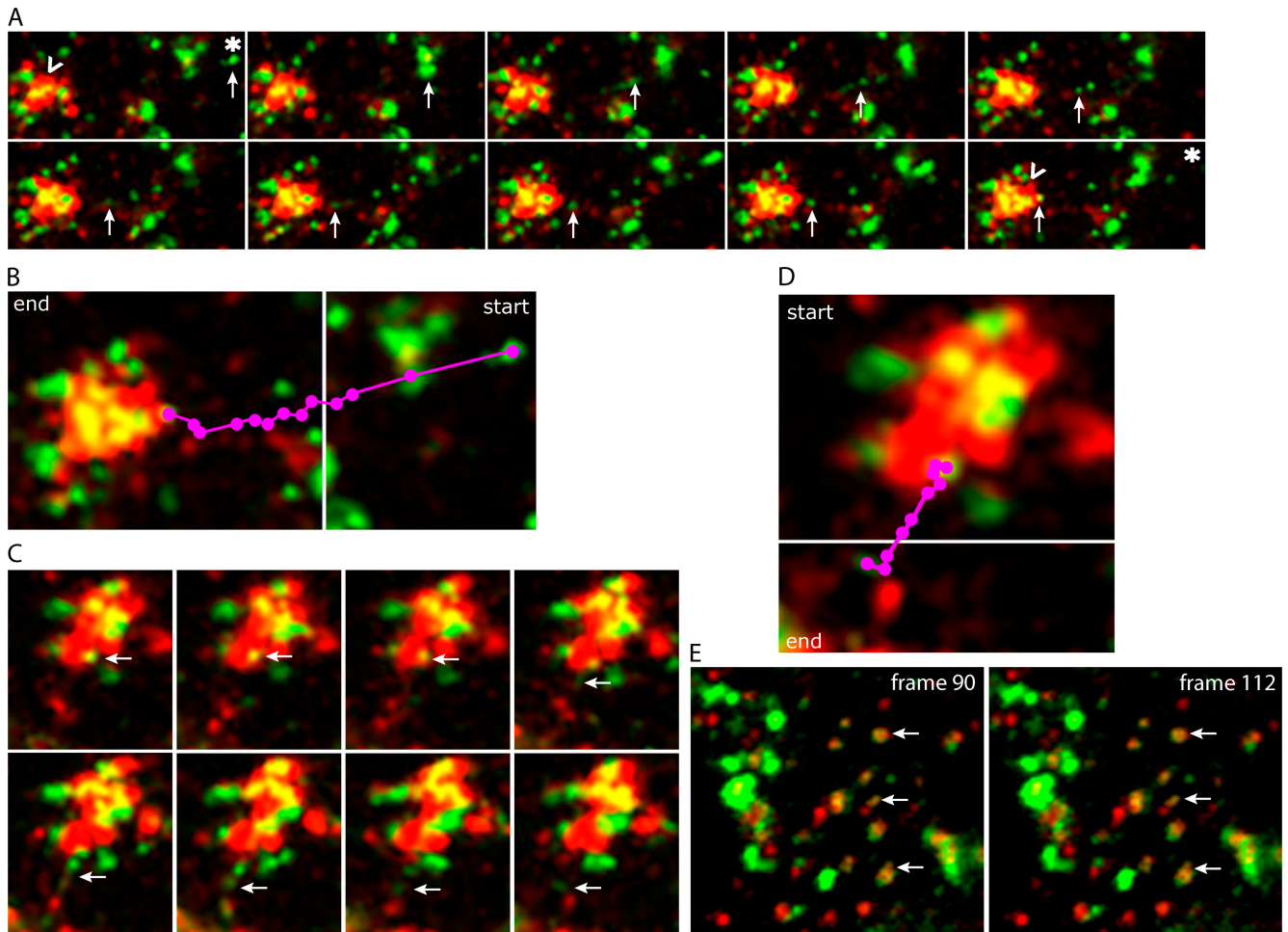
Figure 2. **VSV-G is transported directly to and from REs as visualized by time-lapse microscopy.** See Online supplemental material for original video images, available at http://www.jcb.org/cgi/content/full/jcb.200408165/DC1. (A) Individual frames from a movie of cells as prepared in Fig. 1 that were imaged immediately upon release of the TGN block by incubation at 31°C. Images were taken every 7 s for 30 min. Frame sequence illustrates the entry of VSV-G (green structures denoted by arrows; the asterisk marks starting point) into Tfn+ (red) RE structures. Note the increase of VSV-G in REs over the time course of these images, indicated by the increase in yellow (noted by "carrots" in the first and last frames). (B) Purple dots denote the path followed by VSV-G from the first frame (start) to the last frame in the sequence illustrated in A (end). (C) Sequence of VSV-G exit from REs, showing the apparent generation of a green VSV-G tubule and resulting vesicles from a yellow structure contained within the red RE region (arrows). Time course is the same as in A. (D) Purple dots denote the path of VSV-G exit from first frame (start) to last frame (end) in the sequence illustrated in panel C. (E) Image of cell periphery from a cell prepared as in A. Images were taken every 7 s. Arrows denote colocalization of VSV-G with Tfn, an association that was maintained >2.5 min, suggesting that the VSV-G and Tfn were contained within the same structure or reflected two distinct but tethered structures.

cell imaging experiments, each marker was visualized with antibodies to GFP and Alexa 488, respectively.

As expected, in cells maintained at 20°C, VSV-G was found mainly in the Golgi complex, present throughout the cisternal elements and not just the TGN (Fig. 3, A and B, arrows denote VSV-G, 5 nm gold). Some staining was also observed in Golgi-associated vesicles and electron-lucent structures. These structures included endosomes that were positively labeled for Tfn (labeled e in Fig. 3, A and B; 10 nm gold), which had been internalized for 2 h at 20°C. Tfn was absent from the Golgi complex per se. Accordingly, the bulk of VSV-G was present in elements of the Golgi complex at 20°C, with only a small amount found in Tfn+ endosomes.

After releasing the cells from the 20°C block by incubation for 10 min at 31°C, a substantial amount of the VSV-G now colocalized with Tfn in endocytic structures (Fig. 3, C and

D, arrows denote VSV-G; 5 nm gold). Structures positive for both Tfn and VSV-G were pleiomorphic, often consisting of anastomosing tubules and vesicles and multivesicular elements. These are the morphological hallmarks of REs in MDCK cells.

Because some VSV-G labeling could be detected on endosomes at 20°C, we compared the extent of colocalization of VSV-G and Tfn at the two temperatures by stereology. For this purpose, we estimated the density of labeling for VSV-G on endosomes that were sampled on random micrographs and defined by the presence of Tfn (see Materials and methods). Upon incubation at 31°C, the density of VSV-G labeling on Tfn+ endosomes increased approximately fourfold, whereas the linear density of labeling for Tfn remained constant (Fig. 3 E). A simpler way to express these results is to calculate the ratio of number of gold particles labeling VSV-G in endosomes over
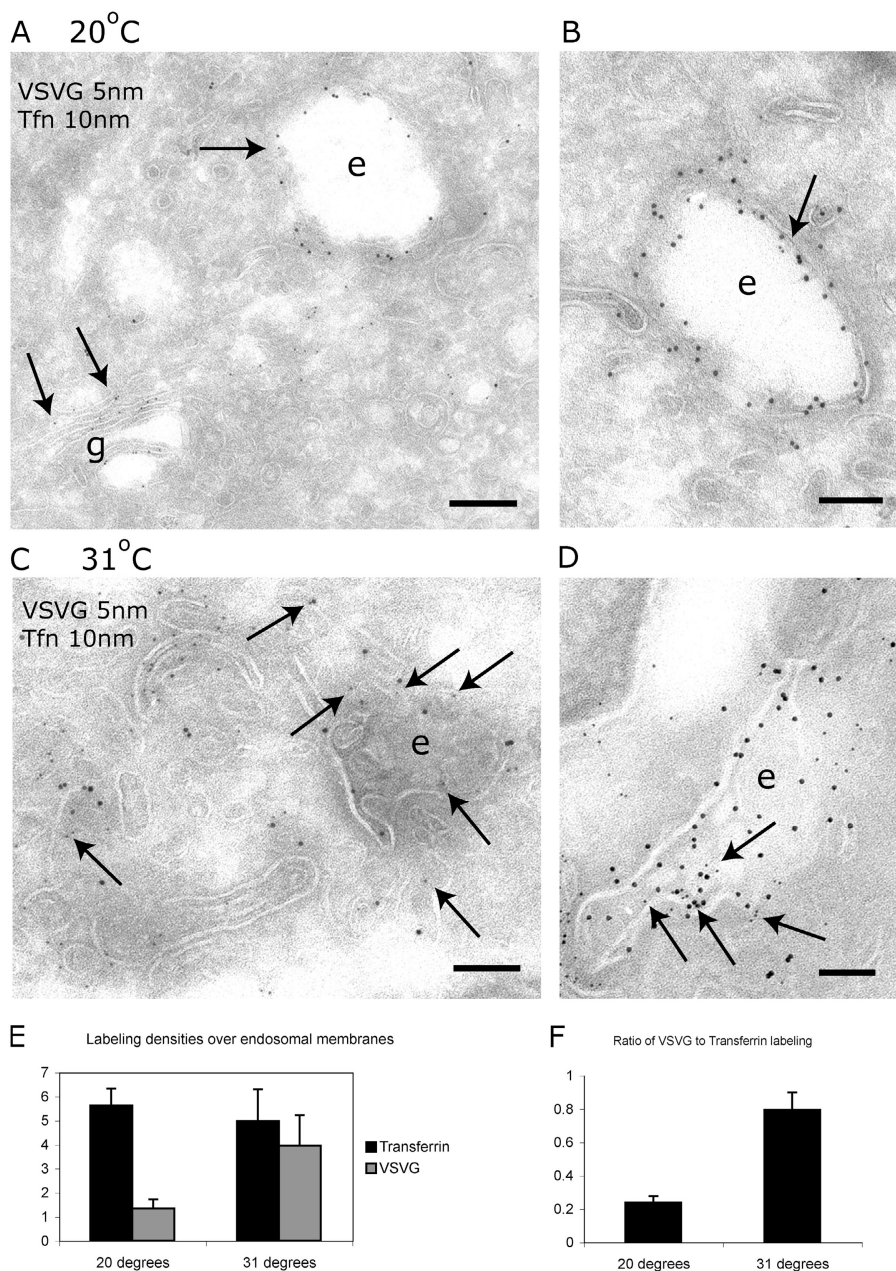
A 20°C

VSVG 5nm
Tfn 10nm

e

g

B

e

C 31°C

VSVG 5nm
Tfn 10nm

e

D

e

E Labeling densities over endosomal membranes

■ Transferrin
□ VSVG

20 degrees   31 degrees

F Ratio of VSVG to Transferrin labeling

20 degrees   31 degrees

Figure 3. **VSV-G and Tfn colocalize in endosomes by immuno-EM.** (A and B) Immuno-EM of MDCKT cells expressing VSV-G-YFP and having endocytosed Alexa 488-Tfn after 2-h incubation at 20°C. VSV-G (5 nm gold, arrows) was localized to the Golgi complex, peripheral vesicles, and, occasionally, on endosomes (arrow on "e"). Tfn (10 nm gold) was localized to endosomes (e). Bars: (A) 200 nm; (B) 100 nm. (C and D) Immuno-EM of MDCKT cells released from the 20°C TGN block by incubation at 31°C for 10 min. VSV-G (5 nm gold, arrows) and Tfn (10 nm gold) were localized to the same endosomal compartments (e). Bars, 100 nm. (E) Labeling density of VSV-G on Tfn+ endosomes. Density of VSV-G labeling increases fourfold during 31°C incubation. (F) Ratio of number of gold particles labeling VSV-G in endosomes over the number of gold particles labeling Tfn. Error bars represent the SD of labeling density from three grids.

Downloaded from http://rupress.org/jcb/article-pdf/167/3/531/1870249/jcb1673531.pdf by guest on 24 April 2024

the number labeling Tfn. When expressed this way, the results also revealed a fourfold increase on incubation at 31°C (Fig. 3 F). Thus, upon exit from the TGN, at least a fraction of VSV-G entered into Tfn-positive endosomes.

Immunoisolated VSV-G–positive structures contain Tfn after VSV-G exit from the TGN

To further characterize the encounter between newly synthesized VSV-G and internalized Tfn, we turned to an independent biochemical approach, immunoisolation. Using an optimized magnetic bead-based method (Taguchi et al., 2003), we used an immobilized anti-GFP polyclonal antibody to capture membranes containing YFP-tagged VSV-G from MDCKT cell lysates. The converse experiment, using GFP-tagged TfnR,

proved impossible because the addition of a cytoplasmic domain GFP altered the transport and intracellular localization of the receptor.

Cells were infected with a recombinant adenovirus encoding VSV-G-YFP and incubated overnight at 40°C. Alexa 488-Tfn was added to the medium for 2 h, with the cells either maintained at 40°C (to retain VSV-G-YFP in the ER) or shifted to 20°C. The 20°C cultures were either harvested or shifted to 31°C for 10 min and then harvested. Postnuclear supernatants were prepared and VSV-G-YFP+ membranes were captured by magnetic-bead immobilization. Captured membranes were assayed for Alexa 488-Tfn by quantitative Western blot.

In a representative SDS-PAGE gel from four separate experiments, Fig. 4 A shows that relatively little Tfn was detected with VSV-G+ membranes isolated during the 40°C ER block.
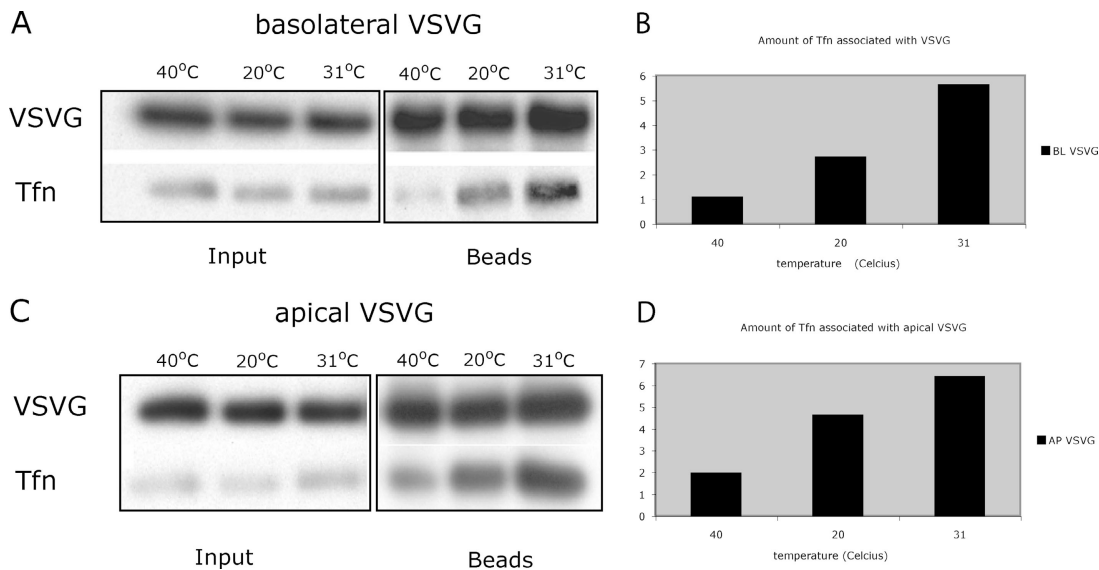
RECYCLING ENDOSOMES IN SECRETORY TRAFFIC • ANG ET AL.   535

Figure 4. Immunoisolated VSV-G membranes from MDCKT are associated with Tfn after exit from the TGN. (A) Representative Western blot of immunoisolated basolateral VSV-G-YFP containing membranes from VSV-G-YFP–infected MDCKT cells incubated with Alexa 488-Tfn during a 40°C ER block, 20°C TGN block, and 10-min chase at 31°C. Immunoprecipitation of VSV-G was performed using magnetic beads coupled to anti-GFP antibody (beads lanes) and probed for VSV-G (VSV-G row). VSV-G purified membranes were also probed for the presence of Alexa 488-Tfn using anti–Alexa 488 antibody (Tfn lane). This is a representative blot from four experiments. (C) Same as in A but apical mutant VSV-G-G3-YFP was used; representative blot from three experiments. (B and D) Quantification of Tfn associated with VSV-G under the three temperature conditions from A and B.

In contrast, more Tfn was coimmunoprecipitated with VSV-G membranes isolated following the 20°C chase and, especially, following the 31°C chase. The total recovery of VSV-G isolated at each time point was identical. These results were quantified by image digitization, demonstrating that relative to the amount of Tfn coprecipitated at 40°C, the efficiency of Tfn coprecipitation increased 2.5-fold after the 20°C shift and 5.5-fold after the 31°C shift (Fig. 4 B). These data were consistent with the immuno-EM experiments, which showed a greater than fourfold increase in VSV-G and Tfn colocalization upon release of the 20°C block (Fig. 3).

At longer times of chase at 31°C (1.5–2 h; Tfn present throughout the chase), very little Tfn was coimmunoprecipitated with VSV-G+ membranes; however, the total amount of VSV-G captured was also much lower (approximately fourfold; unpublished data). These results indicated that immunoisolation was less efficient after insertion of the VSV-G into the plasma membrane. They also reemphasized that the coprecipitation of Tfn seen at 10 min of chase was not due to VSV-G internalized from the cell surface.

Similar results were obtained when these experiments were performed using the apical VSV-G mutant in place of the basolaterally targeted "wild type" (Fig. 4, C and D). Here, however, a somewhat greater amount of Tfn was coimmunoisolated already upon shifting to 20°C.

Together, these data indicate that exit of VSV-G from the secretory pathway placed it in membranes that were physically associated or fused with Tfn-containing REs. That some coprecipitation was observed at 20°C might reflect the "leakiness" of the temperature inhibition suggested by the immuno-EM experiments discussed earlier. Such leakiness might be expected in the case of a temperature block, which is merely a kinetic in-

hibition of a given transport step. Because the efficiency of immunoisolation may not be a linear function of VSV-G concentration, even a small amount of VSV-G in a Tfn-containing endosome may lead to immunoisolation. It is also possible that at 20°C a portion of the Tfn signal resulted from RE- and TGN-derived membranes being tethered or aggregated. Although we could not completely eliminate this possibility, salt-washing or latrunculin B treatment, expected to disperse actin-dependent aggregates, did not reduce the amount of Tfn coimmunoisolated (unpublished data). Moreover, the EM-immunocytochemistry clearly documented that at least some VSV-G and Tfn were contained within common membranes, presumably REs.

RE inactivation caused accumulation of VSV-G in the perinuclear region

Although the aforementioned data suggested that VSV-G was transported through RE before reaching the cell surface, it was not clear if transport through RE was obligatory or what fraction of VSV-G might encounter endosomes. Therefore, we devised an approach to selectively inactivate the RE compartment by making use of the ability of HRP to react with DAB and H_2O_2 to form an insoluble precipitate. A variation of this general strategy had previously been developed to modify or to inactivate the function of the general endosome population (Stoorvogel et al., 1988; Futter et al., 1995; Pond and Watts, 1997). MDCKT cells were allowed to internalize Tfn covalently coupled to HRP (Tfn-HRP) under conditions that resulted in its predominant accumulation in REs (Sheff et al., 1999), thus only Tfn-containing REs (and to some extent early endosomes) would be affected.

VSV-G–expressing MDCKT cells, incubated at 40°C to retain VSV-G in the ER, were allowed to internalize Tfn-HRP,
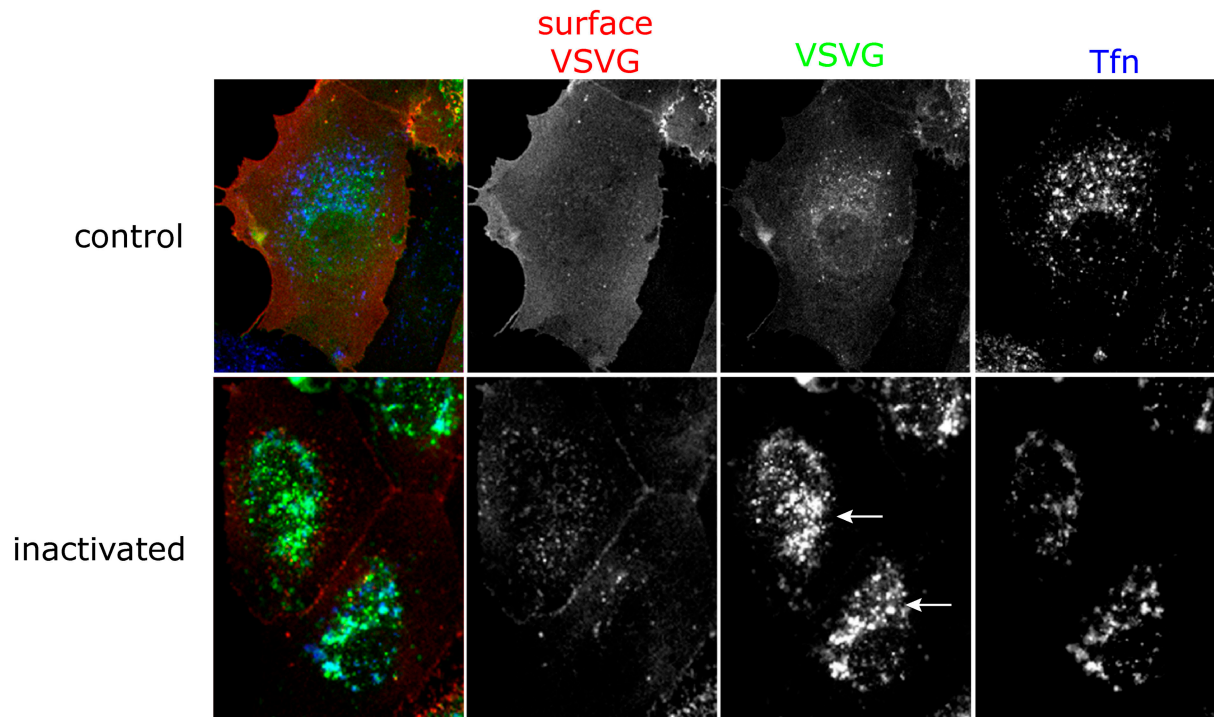
Figure 5. **Inactivation of REs causes accumulation of VSV-G in the perinuclear region.** MDCKT cells were infected to express VSV-G-YFP (third column, green) and incubated overnight at 40°C. Tfn-HRP (third column, blue) was internalized for 45 min at 40°C and was chased into REs by incubating cells in media without Tfn-HRP for 15 min at 40°C. Control cells were subject to only DAB while the samples were exposed to DAB and H_2O_2 for 1 h in the dark. Cells were washed in warm media and incubated at 31°C for 1.5 h in media/CHX to release VSV-G from the ER. Cells were washed in PBS^{cmf}, trypsinized, fixed, and processed for immunofluorescence. Cell surface VSV-G labeling (second column, red) using an antibody, TKG, against the ectodomain of VSV-G was performed on nonpermeabilized cells before permeabilization and internal labeling for HRP. Arrows denote accumulation of intracellular VSV-G in the perinuclear region.

and then were treated with DAB and H_2O_2 on ice for 1 h. The reaction was stopped and the cells incubated at 31°C to release VSV-G from the ER and allow its transport through the Golgi complex and on to the cell surface. The 20°C block was omitted for these experiments. Cycloheximide (CHX) was included during the chase to prevent new VSV-G synthesis. The cells were analyzed for the presence of VSV-G at the cell surface using a monoclonal antibody (TKG) against the ectodomain of VSV-G on nonpermeabilized cells. Under control conditions, i.e., adding DAB without H_2O_2, most of the VSV-G was transported to the plasma membrane after 1.5 h of chase, as there was strong labeling of surface VSV-G and relatively little GFP fluorescence intracellularly (Fig. 5, top; red, surface VSV-G; green, VSV-G; blue, Tfn). However, upon RE inactivation (cells treated with DAB plus H_2O_2), a considerable amount of VSV-G-GFP was now found in the perinuclear region (Fig. 5, arrows). The intracellular VSV-G-GFP at least partially colocalized with Tfn-HRP, suggesting that it had been trapped in inactivated REs. There appeared to be much less VSV-G at the cell surface, although some surface VSV-G was indicated by the lateral staining between cells (Fig. 5, second column, red). Further controls demonstrated that inhibition of VSV-G transport was not observed if cells had not been exposed to Tfn-HRP but were still treated with DAB plus H_2O_2 (unpublished data).

To ensure that the VSV-G trapped intracellularly was blocked on the way out, we performed a time course in which cells were assayed for surface and total VSV-G at various times after the inactivation step. As shown in Fig. 6, in control cells (Fig. 6 A) the expected ER-like pattern of intracellular VSV-G became a more punctate Golgi-endosomal pattern within 30 min after shifting from 40 to 31°C, although surface VSV-G was not detected until 60–90 min. In cells subjected to DAB inactivation before the temperature shift (Fig. 6 B), the intracellular punctate pattern again appeared within 30 min, and remained in most cells for the remainder of the chase. As expected, little VSV-G appeared at the plasma membrane, with this occurring largely in cells that failed to accumulate VSV-G intracellularly (Fig. 6 B, asterisk). Such cells either did not take up Tfn-HRP initially or, more likely, reversed the DAB inactivation because surface VSV-G was only observed at long chase times (>120 min).

Thus, intracellular retention of VSV-G in the inactivated cells occurred long before surface appearance of VSV-G, strongly suggesting that the block occurred on the secretory pathway, rather than following endocytosis of VSV-G that had already reached the surface.

Inactivation of REs inhibited cell surface arrival of VSV-G

Although the aforementioned data revealed a clear intracellular retention of VSV-G following RE inactivation, we were unable to quantify the extent to which cell surface transport was inhib-
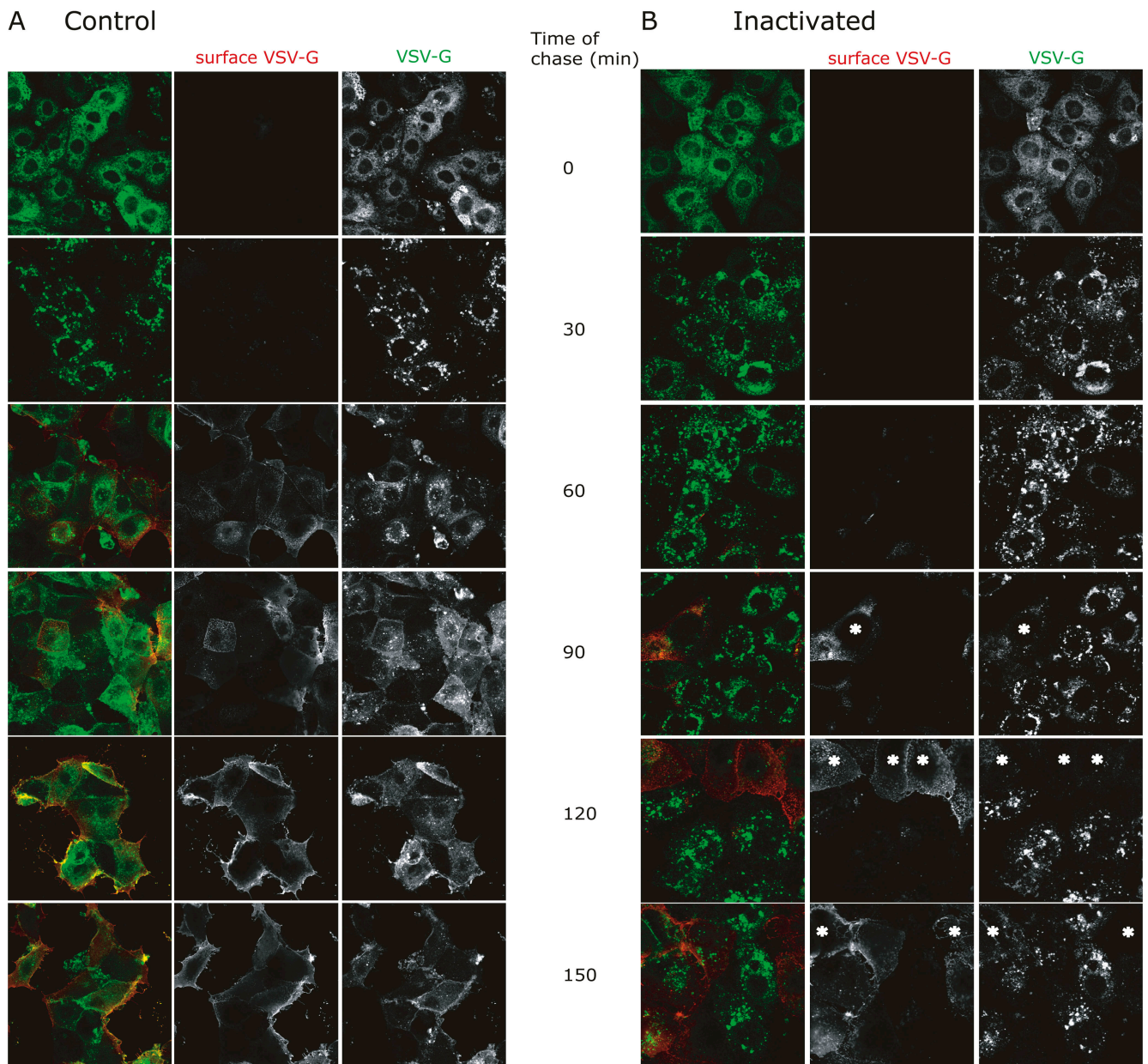
Figure 6. Inactivation of RE caused an inhibition of VSV-G transport in the secretory pathway. MDCKT cells were prepared identically as in Fig. 5 but processed for immunofluorescence every 30 min up to 2.5 h total time of chase at 31°C. Peroxide was not present in control cells (A), whereas samples whose REs were inactivated were subject to peroxide (B). Cells in B that apparently escaped the DAB inactivation at long times of chase are marked by asterisks. Red, surface VSV-G (TKG staining); green, total VSV-G fluorescence.

ited by immunofluorescence alone. Therefore, based on the immunofluorescence time course data, flow cytometry was performed on nonpermeabilized cells that had been labeled for surface VSV-G using the TKG monoclonal antibody after 90 min of chase (Ang et al., 2003). This assay not only allowed quantitative assessment of thousands of cells, but allowed the surface appearance results to be directly correlated with the total amount of VSV-G-GFP expressed (by gating on GFP fluorescence). Representative flow cytometry results were presented as dot plots showing the percentage of cells analyzed for levels of surface VSV-G (y-axis) expression as a function of total VSV-G expression levels (x-axis). The level of Tfn-HRP

uptake, detected by intracellular immuno-labeling of HRP also detected by flow cytometry, was found to be comparable in both control and experimental conditions (unpublished data).

As shown in Fig. 7 A (taken from a representative experiment performed in triplicate), under control conditions, where MDCKT cells have internalized Tfn-HRP but were not subject to the DAB-peroxidase reaction (omitting DAB, Tfn-HRP, or H_2O_2; described for Fig. 5, top; and Fig. 6 A), nearly all of the VSV-G-GFP–expressing cells successfully transported VSV-G to the cell surface (Fig. 7 A, control, top panels). The majority of the cells appeared in quadrant II, indicating that they were positive for both surface and total VSV-G-GFP. How-
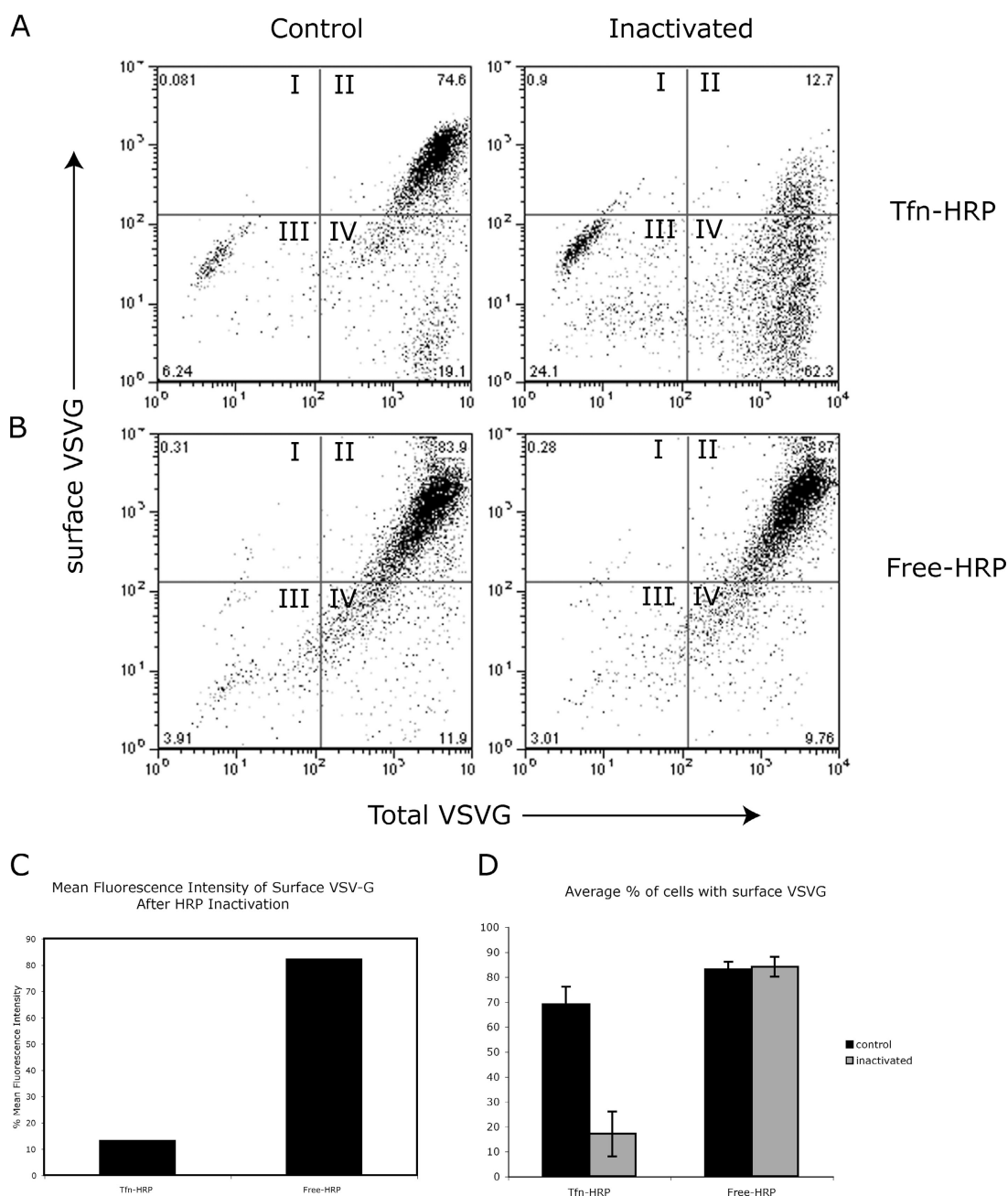
Figure 7. **Inactivation of membranes containing Tfn-HRP, but not free-HRP, inhibited the cell surface arrival of VSV-G.** (A) Representative dot plot of flow cytometry results from cells prepared as in Fig. 5 (Tfn-HRP). Levels of surface VSV-G, performed on nonpermeabilized cells using the TKG antibody, were quantified on the y-axis whereas total VSV-G, as monitored by YFP fluorescence, was quantified on the x-axis. Cells in quadrant I were positive for only surface VSV-G, cells in quadrant II were positive for both surface and total VSV-G, cells in quadrant III were negative for both markers, and cells in quadrant IV were negative for surface VSV-G and positive for total (i.e., intracellular) VSV-G. Numbers in corners represent percentage of cells in that quadrant. (B) MDCKT cells expressing VSV-G-YFP were incubated with free-HRP followed by chase in HRP-free media to load HRP into lysosomes (Free-HRP). Control cells were incubated with DAB alone while the "inactivated" set was incubated with DAB plus H_2O_2 for 1 h in the dark. (C) Percentage MFI of surface VSV-G was measured in cells that were positive for total VSV-G (all cells in quadrants II and IV) and had Tfn-HRP– or free-HRP–containing compartments inactivated. MFI was normalized based on levels in control cells. (D) Average percentage of cells based on three experiments performed in triplicate with surface VSV-G after an uptake of Tfn-HRP or free-HRP under control (black) or inactivation (gray) conditions. Error bars represent the SD from cells with surface VSV-G from three different experiments.

ever, if the DAB reaction was performed to inactivate Tfn-HRP–containing RE compartments before the 31°C chase, <13% of the cells, whose total VSV-G expression level was similar to those of control cells, were able to transport VSV-G to the cell surface (Fig. 7 A, inactivated, quadrant II). Thus,

>60% of the cells containing Tfn-HRP were negative for surface VSV-G expression after RE inactivation (Fig. 7 A, quadrant IV). The mean fluorescence intensity (MFI) of surface VSV-G was also measured for control and inactivated cells whose total VSV-G levels were high, i.e., all cells in quadrants

II and IV. Statistical analysis revealed that the MFI of surface VSV-G of inactivated MDCKT cells was only 15% of that in control cells, suggesting that Tfn-HRP–mediated inactivation of RE inhibited the transport of VSV-G to the cell surface by 85% (Fig. 7 C, Tfn-HRP). Moreover, those inactivated cells that displayed surface VSV-G did so at levels that were reduced relative to controls (Fig. 7, compare quadrant II); this finding is consistent with a partial inhibition or a reversal of the block at long chase times, as suggested in Fig. 6.

To verify that this inhibition was specific to Tfn-HRP–mediated RE inactivation and not due to some general, nonspecific effect of the DAB reaction, the aforementioned experiments were repeated following the endocytosis of non-conjugated HRP (free-HRP), which, when followed by a chase in HRP-free media, accumulates in lysosomes (Steinman et al., 1974). VSV-G-GFP–expressing MDCKT cells were incubated in 0.5 mg/ml free HRP for 12 h at 40°C, conditions that resulted in an accumulation of the same amount of intracellular HRP as had accumulated after Tfn-HRP uptake (quantified by flow cytometry using anti-HRP antibody staining of permeabilized cells; unpublished data). After the DAB reaction ($\pm$ H_2O_2 as a control), the cells were shifted to 31°C and VSV-G chased to the cell surface. In a representative experiment (performed in triplicate) of control cells, as expected, free HRP uptake, without added H_2O_2, had a minimal effect on VSV-G transport to the cell surface (Fig. 7 B, control, quadrant II). >80% of MDCKT cells were able to transport VSV-G-protein to the plasma membrane (Fig. 7 C). Likewise, but in contrast to Tfn-HRP–mediated inactivation, inactivation of free HRP-containing compartments did not affect the transport of VSV-G to the cell surface (Fig. 7 B, inactivated, quadrant II). Again, >80% of the VSV-G–expressing cells were able to transport VSV-G to the cell surface (Fig. 7 B, inactivated, quadrant II). The MFI of cell surface VSV-G after inactivation of free-HRP was close to 80% of that of control cells, suggesting that there was minimal inhibition of VSV-G surface transport.

These results demonstrate that selective inactivation of endosomes by Tfn-HRP greatly reduces the ability of VSV-G protein to be transported from the Golgi complex to the plasma membrane. Thus, MDCKT cells would appear to require a functional RE compartment to transport newly synthesized cargo such as VSV-G to the cell surface.

Discussion

Understanding the relationship between the secretory and endocytic pathways has proved a vexing problem for the last two decades. One clear example is shown by newly synthesized MHC class II-invariant chain complexes (Wolf and Ploegh, 1995). Upon exit from the TGN, the complexes are diverted from the secretory pathway and delivered to one or more endosomal compartments where the class II-invariant chain is proteolytically removed and antigenic peptides are loaded before plasma membrane delivery. At least in dendritic cells, transfer to the surface involves a retrograde pathway from late endosomes and lysosomes (Chow et al., 2002). An analogous series of events characterizes the biosynthetic pathway of lysosomal enzymes, which bind to mannose-6-phosphate receptors in the Golgi complex that mediate transport endosomes, where the enzymes are deposited for eventual transfer to lysosomes (Kornfeld and Mellman, 1989; Puertollano et al., 2001). In both cases, targeting to endosomes reflects the involvement of at least two classes of adaptor complexes, AP-1 and GGA (Puertollano et al., 2001; Zhu et al., 2001). The adaptors recognize targeting signals in the cytoplasmic domain of the receptor, although it remains uncertain if this recognition occurs in the TGN, at a post-TGN site, or both.

Whether "constitutive" transport of secretory cargo or newly synthesized plasma membrane proteins involves an endosomal intermediate has been far less clear. Early work in various cell types suggested that this might be the case, although the evidence was far from complete. By EM-immunocytochemistry, newly synthesized VSV-G protein could on occasion be seen in Tfn-containing structures in fibroblasts, although the amounts observed were very small (Hedman et al., 1987). By cell fractionation in HepG2 hepatocytes, a more significant portion of newly synthesized Tfn-R could be cosedimented with Tfn-gold-laden endosomes at times following the exit of secretory cargo from the TGN (Futter et al., 1995). Cell fractionation was also used to show that newly synthesized asialoglycoprotein receptor-R reached MPR-containing compartments in MDCK cells (Leitinger et al., 1995). Finally, a portion of newly synthesized polymeric Ig receptor may reach an endosomal compartment accessible to HRP and thus subject to density shift after H_2O_2-DAB (Orzech et al., 2000).

Despite these suggestions, the most intriguing of which were from polarized epithelial cells, the nature of the compartments where the presumed interactions took place has remained unclear. Moreover, the actual amount of secretory traffic that passed through endocytic compartments was not established. Recent live cell imaging studies in nonpolarized cells failed to illustrate a clear intersection between transport of new VSV-G and early or late endosomes, labeled by Tfn or FITC-dextran (Hirschberg et al., 1998; Keller et al., 2001). Conceivably, these events were too rare to capture, the experiments were not optimized for this purpose, or the intersection does not occur in nonpolarized cells. Another perspective was reported by Polishchuk et al. (2004), who failed to find sorting of basolateral and certain apical cargo upon TGN exit in MDCK cells, consistent with a post-TGN sorting site, possibly endosomes. This work suggested that the endosomal intermediate may occur after endocytosis but this was only applicable to "raft"-dependent apical proteins. Given that work in yeast clearly indicated an intersection of secretory traffic with endosomes before surface arrival (Harsay and Schekman, 2002), we felt that the issue should be carefully reassessed in animal cells. Because many components essential for AP-1B–dependent basolateral transport in epithelial cells appeared to localize at REs, we focused our attention specifically to this compartment.

We believe it was critical to have optimized the conditions for capturing and increasing the chances of intersection of biosynthetic cargo through REs by using an AP-1B–expressing polarized epithelial cell line that was stably transfected with the gene for the human TfnR, and also by the use of serial temper-

ature blocks to synchronize biosynthetic and endocytic traffic. The 20°C block has been extensively used to inhibit secretory transport to the level of the TGN (Griffiths et al., 1985). Incubation at 20°C is also well known to accumulate endocytic tracers in endosomes by blocking their transfer to lysosomes, but also by slowing recycling from REs (Sheff et al., 1999); no transfer of Tfn to the TGN was observed at 20°C in MDCK cells (Futter et al., 1998). The use of cells expressing the human TfnR was also critical, allowing for efficient Tfn uptake and clear labeling of REs even after a relatively short (2 h) incubation at 20°C. The ability to provide strong labeling of the RE compartment increased the chances of capturing transient intersections of VSV-G and Tfn upon release of the temperature block. Although interposing a 20°C block greatly increased our ability to note an overlap of VSV-G and Tfn, it is important to note that the temperature block was not essential, and in fact was not required to block VSV-G transport when REs were loaded with Tfn-HRP. In this respect, it is interesting that preliminary results suggest that in CHO cells, which do not express AP-1B, a potential RE intermediate was seldom observed by fluorescence microscopy whether or not a 20°C block was used to accumulate VSV-G-GFP in the Golgi. This observation suggests the interesting possibility that the RE pathway may not be as prevalent in nonpolarized cells.

The function and identity of REs has been elusive for many years. That they represent a distinct population from early endosomes is reasonably well established, as RE are reached by endocytic tracers such as Tfn with distinct kinetics and have a distinct Rab GTPase profile, being enriched, for example, in Rab11 (Ullrich et al., 1996; Daro et al., 1997; Sonnichsen et al., 2000). They are often, but not always, found in the perinuclear cytoplasm. REs are generally thought to comprise an intracellular pool of components that can be recruited to the plasma membrane in response to specific stimuli, such as during phagocytosis or cell migration (Mellman, 2000).

In epithelial cells, several lines of evidence have suggested that REs may play a role in the polarized sorting of receptors internalized during endocytosis. During transcytosis of pIgR or TfnR, microscopy has revealed transient residence of transcytotic markers in perinuclear endosomes in the apical cytoplasm, possibly RE (Casanova et al., 1999; Sheff et al., 1999; Orzech et al., 2000; Wang et al., 2001). These structures also appeared to contain AP-1 adaptors (Futter et al., 1998). Of further interest is the suggestion that REs in MDCK cells are the primary site of signal-dependent sorting during polarized recycling (Sheff et al., 1999). Such sorting may involve the AP-1B complex (Gan et al., 2002).

That REs may serve as a hub for the sorting of newly synthesized and endocytosed proteins is consistent with the finding that, thus far, REs have been the only site to which the known components of the polarized sorting and transport machinery are recruited. These include AP-1B, Rab8, and at least two exocyst subunits (Ang et al., 2003; Fölsch et al., 2003). Until now, the presence of these components in REs suggested their role only in polarized recycling. It now seems likely that at least some newly synthesized VSV-G protein may reach REs before appearing at the plasma membrane. The rapid kinetics

of transfer to REs demonstrated that it can occur immediately upon TGN exit, as there was insufficient time for the VSV-G to transit via the cell surface. The DAB inactivation experiments further suggested that the large majority of new VSV-G protein must pass through a compartment also accessible to Tfn-HRP in order to arrive at the cell surface. HRP inactivation reduced VSV-G transport by >85%. Although we have not definitively characterized the compartment(s) responsible for this inhibition, REs seem a likely candidate based on the fact that inhibition was only observed using the RE-selective probe, Tfn-HRP, although we cannot exclude the possibility that other compartments (early endosomes) might also be involved. Loading cells with an enzymatically equivalent amount of free HRP, found largely in lysosomes, had no effect on the transport of VSV-G. Other attempts to inactivate REs have been consistent with these results, albeit less clear. Expression of a constitutively activated Rab8 mutant, an RE-associated GTPase, inhibited basolateral sorting by preventing AP-1B recruitment, although it did not block overall (nonpolarized) transport to the surface (Ang et al., 2003). Expression of dominant-negative Rab11, at least in fibroblasts, caused a small but reproducible inhibition of VSV-G transport (Chen et al., 1998). Because the effect of dominant-negative Rab11 on Tfn recycling to the cell surface is also slight (Wilcke et al., 2000), this, however, may not be an effective means to inactivate REs.

Our results provide the most direct evidence yet that REs play a role on the biosynthetic pathway of plasma membrane proteins. Although more work will be required to establish the functional significance of the endosomal intermediate, and other cargoes must be evaluated before generalizations are possible, it is attractive to predict that its purpose in epithelial cells is to provide a site for sorting apical and basolateral proteins. This role was indirectly suggested by the presence of functionally important elements of the AP-1B–dependent basolateral pathway in REs. Endosomes are well known to be capable of polarized sorting, particularly in hepatocytes and colonic epithelium (Bartles et al., 1987; Matter et al., 1993). In hepatocytes, little sorting occurs in the biosynthetic pathway, with many apical and basolateral proteins delivered together to the basolateral surface, being sorted after internalization and transfer to endosomes. Viewed in this context, it is reasonable to imagine that epithelial cells concentrate components of their machinery for polarized sorting to a single site on both the endocytic and secretory pathways.

Materials and methods

Cell culture
MDCK-TfnR (MDCKT) stable cells were maintained in Dulbecco's MEM (10% FBS) plus 0.5 g/ml geneticin as described previously (Sheff et al., 1999).

Tfn uptake
MDCKT cells grown on coverslips were induced with 10 mM butyrate 16 h before Tfn uptake. Alexa 546-Tfn, Alexa 488-Tfn (Sigma-Aldrich), or Tfn-HRP (HRP; Accurate Biochemical; US Biological) was used. For immunofluorescence or live cell imaging, coverslips were preincubated in serum-free media for 30 min at 40°C to deplete Tfn. Cells were inverted onto droplets of 100 µg/ml Tfn-546 on ice for 30 min, and then incubated at 20°C for 2 h in media/10 mM Hepes, with the last hour in me-

dia plus CHX. Cells were incubated at 31°C in for VSV-G export. Immuno-fluorescence or video microscopy was performed as described in the section Live confocal microscopy.

Recombinant adenoviruses
The ts045 VSV-G-YFP and apical variant were gifts from P. Keller (University of Heidelberg, Heidelberg, Germany; Keller et al., 2001). All infections were performed 24 h before analysis of the proteins either by immunofluorescence or FACS. MDCKT cells were infected at 4 PFU per cell and incubated at 40°C overnight. Propagation and generation of recombinant adenoviruses were performed as described in the pAdeasy vector protocol (Qbiogene).

Immunofluorescence microscopy
Immunofluorescence microscopy was performed as described previously (Ang et al., 2003).

Antibodies
Antibodies used were anti-VSV-G, TKG, for VSV-G surface labeling (obtained from the late T. Kreis, University of Geneva, Geneva, Switzerland), anti-GFP (provided by G. Warren, Yale University, New Haven, CT), and anti-HRP (Transduction Laboratories).

Live confocal microscopy
Coverslip-grown MDCKT cells were infected with ts045 VSV-G-YFP and induced with 5 mM butyrate for 16 h at 40°C. Tfn uptake was performed as described above. Cells were incubated 2 h in media at 20°C (last hour in media plus 0.1 mg/ml CHX). Coverslips were transferred to a heated (37°C) chamber (Tempcontrol Digital 37–2 device; Warner Instruments) cell-side down to a warm 35-mM glass-bottom dish (Mat-Tek Co.) with media/CHX and imaged immediately on a confocal microscope (model LSM 510; Carl Zeiss MicroImaging, Inc.) with a 40× 1.4 NA Plan-Apochromat water-immersion lens. Acquisition was performed using LSM 510 version 3.0 software (Carl Zeiss MicroImaging, Inc.) and processed with Adobe Photoshop 7.0 and Volocity (Improvision) 2.0.1 software. Movies were assembled using Graphic Converter version 3.8.

Immunoisolation of VSV-G-YFP–containing membranes
MDCKT cells (2 × 10-cm dishes) were washed twice with PBS, once with homogenization buffer (20 mM Hepes, pH 7.4, 0.25 M sucrose, and protease inhibitors), and scraped into 2 ml of homogenization buffer. Cells were disrupted with a ball-bearing homogenizer (0.01-mm clearance, 16 strokes). Homogenates were subjected to centrifugation (500 g for 5 min) twice. Final supernatant was designated PNS fraction and subsequently used for immunoprecipitation reaction. Immunoprecipitation reaction was done as previously described (Taguchi et al., 2003).

HRP inactivation
Cells were incubated with 0.010 mg/ml Tfn-HRP in media for 45 min or overnight at 40°C, washed once in serum-free DME, and incubated 15 min. Cells were washed twice in ice-cold PBS. Surface-bound Tfn-HRP was removed by two 5-min washes in 0.15 M NaCl and 20 mM of citric acid, pH 5.0. Cells were washed with ice-cold PBS, pH 7.4, and resuspended in PBS containing 0.1 mg/ml DAB (Sigma-Aldrich). H_2O_2 was added to a final concentration 0.025% to the inactivation sample; PBS was added to the control set. Cells were incubated on ice for 60 min in the dark and the reaction was stopped by washing cells twice in PBS/BSA 1%. Warm media/CHX was added and cells were incubated at 31°C. Cells were harvested after washing once in PBS^{cmf} ($-Ca_2$, $-Mg_2$), incubating for 10–15 min in 1 mM trypsin, and collected and fixed in 2% PFA and labeled for surface VSV-G or internalized HRP. To load lysosomal compartments, cells were incubated with 0.5 mg/ml of free HRP (Sigma-Aldrich) overnight at 40°C in MDCKT media. HRP was chased for 1 h in serum-free DME before inactivation.

Flow cytometry analysis
Flow cytometry was performed with FACSCalibur using CellQuest software (Becton Dickinson) for acquisition. Data was analyzed with FloJo (TreeStar). Secondary antibodies were goat anti–mouse phycoerythrin, biotin-conjugated goat anti–rabbit, and streptavidin phycoerythrin (Sigma-Aldrich).

Immuno-EM
Double immuno-EM was performed as described previously (Fölsch et al., 2003) using anti–Alexa 488 and anti-GFP antibodies (both from Molecular Probes, Inc.). Sections were observed in a Tecnai 12 Biotwin electron microscope. For quantitation, three independent grids were analyzed for each temperature condition, and from each grid 25 regions were sampled at random and photographed. Micrographs were printed at a final magnification of 61,000. Labeling densities of both Tfn and VSV-G were estimated on endosomes and related structures by dividing the number of gold particles by the membrane length of these organelles. Membrane length was estimated by counting the number of intersections with a lattice grid with a 5-mm distance between lines. Organelles were identified as endosomes on the basis of their positive labeling for Tfn.

Online supplemental material
Fig. S1 shows localization of VSV-G with Tfn-positive REs in MDCK cells in the absence of the 20°C TGN block. The videos show VSV-G entering and exiting Tfn-positive REs during secretory transport as described in Figs. 1 and 2. Online supplemental material is available at http://www.jcb.org/cgi/content/full/jcb.200408165/DC1.

References

Ang, A.L., H. Fölsch, U.M. Koivisto, M. Pypaert, and I. Mellman. 2003. The Rab8 GTPase selectively regulates AP-1B–dependent basolateral transport in polarized Madin-Darby canine kidney cells. *J. Cell Biol.* 163: 339–350.

Bartles, J.R., H.M. Feracci, B. Stieger, and A.L. Hubbard. 1987. Biogenesis of the rat hepatocyte plasma membrane in vivo: comparison of the pathways taken by apical and basolateral proteins using subcellular fractionation. *J. Cell Biol.* 105:1241–1251.

Bonifacino, J.S., and L.M. Traub. 2003. Signals for sorting of transmembrane proteins to endosomes and lysosomes. *Annu. Rev. Biochem.* 72:395–447.

Casanova, J.E., X. Wang, R. Kumar, S.G. Bhartur, J. Navarre, J.E. Woodrum, Y. Altschuler, G.S. Ray, and J.R. Goldenring. 1999. Association of Rab25 and Rab11a with the apical recycling system of polarized Madin-Darby canine kidney cells. *Mol. Biol. Cell.* 10:47–61.

Chen, W., Y. Feng, D. Chen, and A. Wandinger-Ness. 1998. Rab11 is required for trans-golgi network-to-plasma membrane transport and a preferential target for GDP dissociation inhibitor. *Mol. Biol. Cell.* 9:3241–3257.

Chow, A., D. Toomre, W. Garrett, and I. Mellman. 2002. Dendritic cell maturation triggers retrograde MHC class II transport from lysosomes to the plasma membrane. *Nature.* 418:988–994.

Daro, E., D. Sheff, M. Gomez, T. Kreis, and I. Mellman. 1997. Inhibition of endosome function in CHO cells bearing a temperature-sensitive defect in the coatomer (COPI) component ε-COP. *J. Cell Biol.* 139:1747–1759.

Drubin, D.G., and W.J. Nelson. 1996. Origins of cell polarity. *Cell.* 84:335–344.

Fölsch, H., H. Ohno, J.S. Bonifacino, and I. Mellman. 1999. A novel clathrin adaptor complex mediates basolateral targeting in polarized epithelial cells. *Cell.* 99:189–198.

Fölsch, H., M. Pypaert, P. Schu, and I. Mellman. 2001. Distribution and function of AP-1 clathrin adaptor complexes in polarized epithelial cells. *J. Cell Biol.* 152:595–606.

Fölsch, H., M. Pypaert, S. Maday, L. Pelletier, and I. Mellman. 2003. The AP-1A and AP-1B clathrin adaptor complexes define biochemically and functionally distinct membrane domains. *J. Cell Biol.* 163:351–362.

Futter, C.E., C.N. Connolly, D.F. Cutler, and C.R. Hopkins. 1995. Newly synthesized transferrin receptors can be detected in the endosome before they appear on the cell surface. *J. Biol. Chem.* 270:10999–11003.

Futter, C.E., A. Gibson, E.H. Allchin, S. Maxwell, L.J. Ruddock, G. Odorizzi, D. Domingo, I.S. Trowbridge, and C.R. Hopkins. 1998. In polarized MDCK cells basolateral vesicles arise from clathrin-γ-adaptin-coated domains on endosomal tubules. *J. Cell Biol.* 141:611–623.

Gan, Y., T.E. McGraw, and E. Rodriguez-Boulan. 2002. The epithelial-specific adaptor AP1B mediates post-endocytic recycling to the basolateral membrane. *Nat. Cell Biol.* 4:605–609.

Griffiths, G., and K. Simons. 1986. The trans Golgi network: sorting at the exit

site of the Golgi complex. *Science.* 234:438–443.

Griffiths, G., S. Pfeiffer, K. Simons, and K. Matlin. 1985. Exit of newly synthesized membrane proteins from the trans cisterna of the Golgi complex to the plasma membrane. *J. Cell Biol.* 101:949–964.

Grindstaff, K.K., C. Yeaman, N. Anandasabapathy, S.C. Hsu, E. Rodriguez-Boulan, R.H. Scheller, and W.J. Nelson. 1998. Sec6/8 complex is recruited to cell-cell contacts and specifies transport vesicle delivery to the basal-lateral membrane in epithelial cells. *Cell.* 93:731–740.

Harsay, E., and R. Schekman. 2002. A subset of yeast vacuolar protein sorting mutants is blocked in one branch of the exocytic pathway. *J. Cell Biol.* 156:271–285.

Hedman, K., K.L. Goldenthal, A.V. Rutherford, I. Pastan, and M.C. Willingham. 1987. Comparison of the intracellular pathways of transferrin recycling and vesicular stomatitis virus membrane glycoprotein exocytosis by ultrastructural double-label cytochemistry. *J. Histochem. Cytochem.* 35:233–243.

Hirschberg, K., C.M. Miller, J. Ellenberg, J.F. Presley, E.D. Siggia, R.D. Phair, and J. Lippincott-Schwartz. 1998. Kinetic analysis of secretory protein traffic and characterization of Golgi to plasma membrane transport intermediates in living cells. *J. Cell Biol.* 143:1485–1503.

Keller, P., D. Toomre, E. Diaz, J. White, and K. Simons. 2001. Multicolour imaging of post-Golgi sorting and trafficking in live cells. *Nat. Cell Biol.* 3:140–149.

Kornfeld, S., and I. Mellman. 1989. The biogenesis of lysosomes. *Annu. Rev. Cell Biol.* 5:483–525.

Leitinger, B., A. Hille-Rehfeld, and M. Spiess. 1995. Biosynthetic transport of the asialoglycoprotein receptor H1 to the cell surface occurs via endosomes. *Proc. Natl. Acad. Sci. USA.* 92:10109–10113.

Matter, K., W. Hunziker, and I. Mellman. 1992. Basolateral sorting of LDL receptor in MDCK cells: the cytoplasmic domain contains two tyrosine-dependent targeting determinants. *Cell.* 71:741–753.

Matter, K., J.A. Whitney, E.M. Yamamoto, and I. Mellman. 1993. Common signals control low density lipoprotein receptor sorting in endosomes and the Golgi complex of MDCK cells. *Cell.* 74:1053–1064.

Mellman, I. 2000. Quo vadis: polarized membrane recycling in motility and phagocytosis. *J. Cell Biol.* 149:529–530.

Mostov, K.E., M. Verges, and Y. Altschuler. 2000. Membrane traffic in polarized epithelial cells. *Curr. Opin. Cell Biol.* 12:483–490.

Odorizzi, G., A. Pearse, D. Domingo, I.S. Trowbridge, and C.R. Hopkins. 1996. Apical and basolateral endosomes of MDCK cells are interconnected and contain a polarized sorting mechanism. *J. Cell Biol.* 135:139–152.

Ohno, H., T. Tomemori, F. Nakatsu, Y. Okazaki, R.C. Aguilar, H. Foelsch, I. Mellman, T. Saito, T. Shirasawa, and J.S. Bonifacino. 1999. μ1B, a novel adaptor medium chain expressed in polarized epithelial cells. *FEBS Lett.* 449:215–220.

Orzech, E., S. Cohen, A. Weiss, and B. Aroeti. 2000. Interactions between the exocytic and endocytic pathways in polarized Madin-Darby canine kidney cells. *J. Biol. Chem.* 275:15207–15219.

Polishchuk, R., A.D. Pentima, and J. Lippincott-Schwartz. 2004. Delivery of raft-associated, GPI-anchored proteins to the apical surface of polarized MDCK cells by a transcytotic pathway. *Nat. Cell Biol.* 6:297–307.

Pond, L., and C. Watts. 1997. Characterization of transport of newly assembled, T cell-stimulatory MHC class II-peptide complexes from MHC class II compartments to the cell surface. *J. Immunol.* 159:543–553.

Puertollano, R., R.C. Aguilar, I. Gorshkova, R.J. Crouch, and J.S. Bonifacino. 2001. Sorting of mannose 6-phosphate receptors mediated by the GGAs. *Science.* 292:1712–1716.

Rindler, M.J., I.E. Ivanov, H. Plesken, and D.D. Sabatini. 1985. Polarized delivery of viral glycoproteins to the apical and basolateral plasma membranes of Madin-Darby canine kidney cells infected with temperature-sensitive viruses. *J. Cell Biol.* 100:136–151.

Sheff, D.R., E.A. Daro, M. Hull, and I. Mellman. 1999. The receptor recycling pathway contains two distinct populations of early endosomes with different sorting functions. *J. Cell Biol.* 145:123–139.

Sonnichsen, B., S. De Renzis, E. Nielsen, J. Rietdorf, and M. Zerial. 2000. Distinct membrane domains on endosomes in the recycling pathway visualized by multicolor imaging of Rab4, Rab5, and Rab11. *J. Cell Biol.* 149:901–914.

Steinman, R.M., J.M. Silver, and Z.A. Cohn. 1974. Pinocytosis in fibroblasts. Quantitative studies in vitro. *J. Cell Biol.* 63:949–969.

Stoorvogel, W., H.J. Geuze, J.M. Griffith, and G.J. Strous. 1988. The pathways of endocytosed transferrin and secretory protein are connected in the trans-Golgi reticulum. *J. Cell Biol.* 106:1821–1829.

Sugimoto, H., M. Sugahara, H. Fölsch, Y. Koide, F. Nakatsu, N. Tanaka, T. Nishimura, M. Furukawa, C. Mullins, N. Nakamura, et al. 2002. Differential recognition of tyrosine-based basolateral signals by AP-1B subunit μ1B in polarized epithelial cells. *Mol. Biol. Cell.* 13:2374–2382.

Taguchi, T., M. Pypaert, and G. Warren. 2003. Biochemical sub-fractionation of the mammalian Golgi apparatus. *Traffic.* 4:344–352.

Traub, L.M., and G. Apodaca. 2003. AP-1B: polarized sorting at the endosome. *Nat. Cell Biol.* 5:1045–1047.

Ullrich, O., S. Reinsch, S. Urbe, M. Zerial, and R.G. Parton. 1996. Rab11 regulates recycling through the pericentriolar recycling endosome. *J. Cell Biol.* 135:913–924.

Wandinger-Ness, A., M.K. Bennett, C. Antony, and K. Simons. 1990. Distinct transport vesicles mediate the delivery of plasma membrane proteins to the apical and basolateral domains of MDCK cells. *J. Cell Biol.* 111:987–1000.

Wang, E., J.G. Pennington, J.R. Goldenring, W. Hunziker, and K.W. Dunn. 2001. Brefeldin A rapidly disrupts plasma membrane polarity by blocking polar sorting in common endosomes of MDCK cells. *J. Cell Sci.* 114:3309–3321.

Wilcke, M., L. Johannes, T. Galli, V. Mayau, B. Goud, and J. Salamero. 2000. Rab11 regulates the compartmentalization of early endosomes required for efficient transport from early endosomes to the trans-Golgi network. *J. Cell Biol.* 151:1207–1220.

Wolf, P.R., and H.L. Ploegh. 1995. How MHC class II molecules acquire peptide cargo: biosynthesis and trafficking through the endocytic pathway. *Annu. Rev. Cell Dev. Biol.* 11:267–306.

Yeaman, C., K.K. Grindstaff, J.R. Wright, and W.J. Nelson. 2001. Sec6/8 complexes on trans-Golgi network and plasma membrane regulate late stages of exocytosis in mammalian cells. *J. Cell Biol.* 155:593–604.

Zhu, Y., B. Doray, A. Poussu, V.P. Lehto, and S. Kornfeld. 2001. Binding of GGA2 to the lysosomal enzyme sorting motif of the mannose 6-phosphate receptor. *Science.* 292:1716–1718.